Linear theory of multistage forward-wave amplifiers

G. S. Nusinovich and M. Walter
Institute for Plasma Research, University of Maryland, College Park, Maryland 20742-3511
(Received 16 March 1999)

A small-signal theory describing multistage gyro-traveling-wave tubes (gyro-TWTs) is developed. Multistage configurations of gyro-TWTs as well as conventional TWTs seem to be attractive because of their principal ability to operate stably with a high gain, since the stability can be provided by a shortening of each stage while the gain increases with the number of stages. Two regimes of operation, far from cutoff and near cutoff, are considered. In the former case, the equations can be reduced to those describing conventional TWTs and free electron laser amplifiers. Thus a part of the results obtained is also valid for these devices. For two-stage configurations (two waveguides separated by a drift region) the effect of the difference in waveguide cutoff frequencies on the gain and bandwidth is studied. This effect has a common nature with stagger-tuning of cavities, which is widely used in conventional klystrons and gyroklystrons for bandwidth enlargement. The trade-off in gain and bandwidth of such ''stagger-tuned,'' two-stage gyro-TWTs and TWTs is analyzed. Also, the theory of two-stage gyro-TWTs with tapered waveguides and external magnetic field is discussed. [S1063-651X(99)05610-X]

PACS number(s): 52.75.Ms

I. INTRODUCTION

In recent years a strong interest in the development of high-power, large-bandwidth, millimeter-wave amplifiers has been demonstrated. One of the most promising large-bandwidth amplifiers is the gyro-traveling-wave tube (gyro-TWT). As shown in Ref. [1], even in a gyro-TWT with a uniform external magnetic field and constant dimensions of the waveguide in the interaction region, a 10% bandwidth in the *Ka* band at a power level exceeding 10 kW can be realized. However, as has been shown in many experiments, the operation of these tubes can be susceptible to parasitic self-excitation, which very often prevents high-gain, large-bandwidth performance (see, e.g., Refs. [2–4], and references therein).

One of the means to overcome this difficulty is a two-stage configuration, which implies two waveguides separated by a drift section. Each of these waveguides can be sufficiently short for preventing self-excitation. Such a scheme was shown, possibly for the first time, in Ref. [5]. A little later, an analytical study of the bandwidth properties of such a configuration with tapered waveguides was done in Ref. [6]. A much more detailed numerical study of the large-signal operation of these devices was carried out later at the Naval Research Laboratory [7,8]. The studies were followed by successful experimental demonstration of operation in a 20% bandwidth with 25-dB saturated gain [9]. (Note that, in a certain sense, a severed circuit in which a sever is placed inside the waveguide for suppressing parasitic self-excitation [10] can also be treated as a two-stage gyro-TWT.)

In spite of a relatively large number of studies of two-stage gyro-TWTs, a more or less general treatment of these devices, to the best of our knowledge, has not been done yet. In the present paper, we develop a linear theory which describes a small-signal operation of multistage gyro-TWTs with untapered waveguides in the interaction region. Since in the limiting case of dominant inertial bunching the equations describing the gyro-TWT can be reduced to equations describing a conventional TWT, part of our treatment is also valid for linear beam multistage TWTs. Our paper is organized as follows: In Sec. II the equations describing operation far from cutoff and near cutoff are given, and an expression for the small-signal gain is derived. Also in this section, we discuss the formalism describing two-stage gyro-TWTs with tapered waveguides and an external magnetic field. (The derivation of equations describing gyro-TWTs with tapered parameters is given in the Appendix.) In Sec. III we present results of the study. In Sec. IV we discuss our results, and show how the results of the general theory expressed in properly normalized parameters can be used in concrete designs and experiments.

II. GENERAL FORMALISM

In the analysis of interaction between electrons and electromagnetic (EM) waves propagating in a waveguide, we will distinguish two cases: operation far from cutoff, and operation near cutoff. Operation far from cutoff implies that only the forward wave propagates synchronously with electrons, while the backward wave, which may appear due to some reflections of the forward wave from the exit, is nonsynchronous, and, therefore, its interaction with electrons can be neglected. In terms of the cyclotron resonance condition this statement means that for the forward wave the transit angle of electrons,

$$\Theta = (\omega - k_z v_z - s\Omega)\frac{L}{v_z}, \tag{1}$$

does not exceed 2π, while for the backward wave, which has the opposite sign of the Doppler term, $k_z v_z$, this angle is much larger than 2π. This, apparently, corresponds to the condition $|k_z|L \gg 2\pi$, which implies many axial variations of the wave field along the waveguide length L. In Eq. (1) ω and k_z are, respectively, the wave frequency and axial wave

number, and v_z and $s\Omega$ are, respectively, the electron axial velocity and the resonant harmonic of the electron cyclotron frequency.

Operation near cutoff implies the excitation of waves with small axial wave numbers, $|k_z|L \lesssim 2\pi$, when the electrons interact synchronously with both forward and backward waves at the same time. Below, we will consider these two cases separately.

A. Operation far from cutoff

Omitting the derivation of corresponding equations which can be found elsewhere [11,12], let us present these equations in the form describing the changes in the electron energy and phase and in the wave amplitude along the axis of a gyro-TWT operating in a large-signal, stationary regime:

$$\frac{dw}{d\zeta} = -2\frac{(1-w)^{s/2}}{1-bw}\mathrm{Re}(Fe^{-i\theta}), \tag{2}$$

$$\frac{d\theta}{d\zeta} = \frac{1}{1-bw}\{w-\Delta+s(1-w)^{s/2-1}\,\mathrm{Im}(Fe^{-i\theta})\}, \tag{3}$$

$$\frac{dF}{d\zeta} = -I_0\frac{1}{2\pi}\int_0^{2\pi}\frac{(1-w)^{s/2}}{1-bw}e^{i\theta}\,d\theta_0. \tag{4}$$

Here $w=2[(1-h\beta_{z0})/\beta_{\perp 0}^2][(\gamma_0-\gamma)/\gamma_0]$ is the normalized variable describing the changes in electron energy along the axis of the device; $h=k_z c/\omega$ is the normalized axial wave number; β_{z0} and $\beta_{\perp 0}$ are, respectively, the initial axial and orbital velocities of the electrons normalized to the speed of light; γ is the electron energy normalized to the rest energy; and γ_0 is its initial value determined by the beam voltage V_b: $\gamma_0=1+eV_b/mc^2$. In Eqs. (2)–(4), $\zeta=[\beta_{\perp 0}^2(1-h^2)/2\beta_{z0}(1-h\beta_{z0})](\omega z/c)$ is the normalized axial coordinate, parameter $b=h\beta_{\perp 0}^2/2\beta_{z0}(1-h\beta_{z0})$ characterizes the changes in the electron axial velocity with the change in electron energy (the so-called ''recoil effect''), θ is a slowly variable gyrophase of the resonant cyclotron harmonic with respect to the phase of the forward wave $\theta=s(\int_0^\tau \Omega d\tau' + \phi)-(\omega t-k_z z)$ (here ϕ is the gyrophase at the entrance), $\Delta=[2(1-h\beta_{z0})/\beta_{\perp 0}^2(1-h^2)][1-h\beta_{z0}-s(\Omega_0/\omega)]$ is the initial cyclotron resonance mismatch [recall that the term w in figure brackets in Eq. (3) describes the relativistic effect of changes in electron cyclotron frequency due to electron energy modulation], and

$$F = \frac{eA}{mc\omega}\frac{2(1-h\beta_{z0})^2}{\gamma_0\beta_{\perp 0}^3\kappa^3}\frac{\alpha^{s-1}}{(s-1)!2^s}L_s \tag{5}$$

is the normalized wave amplitude for the wave with electric field, $\vec{E}=\mathrm{Re}\{A(z)\vec{E}(\vec{r}_\perp)e^{i(\omega t-k_z z)}\}$. So the axial dependence of the wave envelope $A(z)$ determined by Eq. (4) describes the wave amplification. In Eq. (4),

$$I_0 = 16\frac{eI_b}{mc^3}\frac{1}{h\kappa^2}\frac{(1-h\beta_{z0})^3}{\gamma_0\beta_{\perp 0}^4}\left[\frac{\alpha^{s-1}}{(s-1)!2^s}\right]^2 G_{\mathrm{cpl}} \tag{6}$$

is the normalized beam current parameter (I_b is the beam current). In Eqs. (5) and (6), $\kappa=k_\perp c/\omega=\sqrt{1-h^2}$ is the normalized transverse wave number, $\alpha=k_\perp r_L \simeq s\kappa\beta_{\perp 0}/(1-h\beta_0)$ is the normalized Larmor radius r_L, and

$$L_s=\left[\frac{1}{k_\perp}\left(\frac{\partial}{\partial X}+i\frac{\partial}{\partial Y}\right)\right]^s\Psi(X,Y)$$

is the differential operator describing the transverse structure of the rf Lorentz force acting on electrons with transverse coordinates of a guiding center X and Y; here Ψ is the membrane function which obeys the Helmholtz equation with corresponding boundary conditions [13]. For cylindrical waveguides this function can be written as $\Psi = J_{\pm m}(k_\perp r)\exp(\mp im\varphi)$ where m is the azimuthal index of the wave, and r and φ are the polar coordinates. Correspondingly, $L_s=J_{-(s\mp m)}(k_\perp R_0)\exp[i(s\mp m)\varphi_0]$, where R_0 and φ_0 are polar coordinates of the guiding center, and in Eq. (6) the coupling impedance of a thin annular electron beam to the wave is equal to

$$G_{\mathrm{cpl}} = \frac{J_{m\mp s}^2(k_\perp R_0)}{(\nu^2-m^2)J_m^2(\nu)}. \tag{7}$$

Here $\nu=k_\perp R_w$ (where R_w is the waveguide radius) is the pth root of the equation $J_m'(\nu)=0$, i.e., the eigenvalue for the $\mathrm{TE}_{m,p}$ wave.

Let us emphasize that Eqs. (2)–(4) are valid for any waveguide section of a multistage gyro-TWT. These sections can be characterized by different values of the parameters s, I_0, Δ, and b and, what is most important, the boundary conditions for w, θ, and F are different for different sections. For the normalized energy and phase the boundary conditions at the entrance to each section can be written as $w(\zeta_{\mathrm{in}}^{(n)})$ and $\theta(\zeta_{\mathrm{in}}^{(n)})$ [here (n) is the stage number], which for the input waveguide yield $w^{(1)}(0)=0$, $\theta^{(1)}(0)=\theta_0\in[0;2\pi)$. The boundary condition for the wave amplitude in the input waveguide is $F^{(1)}(0)=F_0$ where F_0 is determined by the input power of a signal (for details, see, e.g., Ref. [14]), in all other well-matched sections $F(\zeta_{\mathrm{in}}^{(n)})=0$. Certainly, in the case of reflections the latter condition should be modified.

In the frame of the small-signal theory, the EM wave causes only small perturbations in electron energy and phase, i.e., in Eqs. (2)–(4) $w=w_{(1)}$ and $\theta=\theta_{(0)}+\theta_{(1)}$. Here subindices (0) and (1) denote zero- and first-order terms, respectively, and $\theta_{(0)}=\theta(0)-\Delta\zeta$. Therefore, linearizing Eqs. (2)–(4) with respect to these perturbations and introducing

$$\tilde{w}=\frac{1}{F_0}\frac{1}{2\pi}\int_0^{2\pi}w_{(1)}e^{i\theta_0}\,d\theta_0,\quad \tilde{\theta}=\frac{1}{F_0}\frac{1}{2\pi}\int_0^{2\pi}\theta_{(1)}e^{i\theta_0}\,d\theta_0,$$

$$\tilde{F}=\frac{F}{F_0}e^{i\Delta\zeta}, \tag{8}$$

one can reduce Eqs. (2)–(4) to the following set of equations:

$$\frac{d\tilde{w}}{d\zeta}=-\tilde{F}, \tag{9}$$

$$\frac{d\tilde{\theta}}{d\zeta}=(1-b\Delta)\tilde{w}+\frac{s}{2i}\tilde{F}, \tag{10}$$

$$\frac{d\tilde{F}}{d\zeta}-i\Delta\tilde{F}=-I_0\left\{i\tilde{\theta}-\left(\frac{s}{2}-b\right)\tilde{w}\right\}. \tag{11}$$

For perturbations $\tilde{w}$, $\tilde{\theta}$, and $\tilde{F}$, whose axial dependence can be given as $\exp(i\Gamma\zeta)$ (where Γ is the wave propagation constant in the presence of the beam), these equations yield the known dispersion equation [11,12,15–17]

$$(\Gamma-\Delta)(\Gamma^2+I_0b)-sI_0\Gamma+I_0=0. \tag{12}$$

As shown in Ref. [18], when the normalized beam current parameter I_0 is small, we can introduce $\gamma=\Gamma/I_0^{1/3}$ and $\delta=\Delta/I_0^{1/3}$, and, ignoring the terms proportional to $I_0^{1/3}$, reduce Eq. (12) to

$$\gamma^2(\gamma-\delta)+1=0, \tag{13}$$

which is the standard dispersion equation for conventional TWTs with negligibly small space charge effects [19]. Note, first, that this normalization corresponds to multiplying the normalized axial coordinate ζ by $I_0^{1/3}$, and, second, that this value $I_0^{1/3}$ and the detuning δ apparently play here the same role as, respectively, the Pierce gain parameter C, and the parameter b in the theory of conventional TWTs [19]. Also note that the transition from Eq. (12) to Eq. (13) corresponds to reducing Eqs. (9)–(11) to

$$\frac{d\tilde{\tilde{w}}}{d\zeta'}=-\tilde{\tilde{F}}, \tag{14}$$

$$\frac{d\tilde{\theta}}{d\zeta'}=\tilde{\tilde{w}}, \tag{15}$$

$$\frac{d\tilde{\tilde{F}}}{d\zeta'}-i\delta\tilde{\tilde{F}}=-i\tilde{\theta}. \tag{16}$$

Here $\zeta'=\zeta I_0^{1/3}$, $\tilde{\tilde{w}}=\tilde{w}/I_0^{1/3}$, and $\tilde{\tilde{F}}=\tilde{F}/I_0^{2/3}$.

Since we are dealing with the cubic dispersion equation (13), which has three roots, we can represent these perturbations as

$$\tilde{\tilde{w}}=\sum_{l=1}^{3}A_le^{i\gamma_l\zeta'},\quad \tilde{\theta}=\sum_{l=1}^{3}B_le^{i\gamma_l\zeta'},\quad \tilde{\tilde{F}}=\sum_{l=1}^{3}C_le^{i\gamma_l\zeta'},$$

and from Eqs. (14) and (15) establish the following relations between coefficients A_l, B_l, and C_l:

$$A_l=\frac{i}{\gamma_l}C_l,\quad B_l=\frac{1}{\gamma_l^2}C_l.$$

Correspondingly, the boundary conditions for the nth stage can be rewritten as

$$i\sum_{l=1}^{3}\frac{1}{\gamma_l^{(n)}}C_l^{(n)}=\tilde{\tilde{w}}(\zeta_{\rm in}'^{(n)}), \tag{17}$$

$$\sum_{l=1}^{3}\frac{1}{\gamma_l^{(n)2}}C_l^{(n)}=\tilde{\theta}(\zeta_{\rm in}'^{(n)}), \tag{18}$$

$$\sum_{l=1}^{3}C_l^{(n)}=\tilde{\tilde{F}}(\zeta_{\rm in}'^{(n)}). \tag{19}$$

Recall that all perturbations are normalized to F_0. Therefore, in the input waveguide, $\tilde{\tilde{F}}(0)=1$.

Equations (17)–(19) form a set of linear inhomogeneous algebraic equations which can easily be solved; i.e., the amplitudes of partial waves $C_l^{(n)}$ can be expressed via the determinant and subdeterminants of these equations. Coefficients in these equations depend on $\gamma^{(n)}$, which are the roots of Eq. (13) for the nth stage. Note that for each successive stage of the device the boundary value for the energy $\tilde{\tilde{w}}^{(n)}(\zeta_{\rm in}^{(n)})$ (here $n\geqslant 2$ is the stage number) is equal to the energy $\tilde{\tilde{w}}^{(n-1)}(\zeta_{{\rm out},w}^{(n-1)})$ at the exit from the previous stage; here $\zeta_{{\rm out},w}^{(n-1)}$ is the normalized distance at which the $(n-1)$st waveguide ends. The boundary condition for the phase $\tilde{\theta}^{(n)}(\zeta_{\rm in}^{(n)})$ takes into account also the effect of ballistic bunching in the drift region between two stages:

$$\tilde{\theta}^{(n)}(\zeta_{\rm in}^{(n)})=\tilde{\theta}^{(n-1)}(\zeta_{{\rm out},w}^{(n-1)})+\tilde{\tilde{w}}^{(n-1)}(\zeta_{{\rm out},w}^{(n-1)})(\zeta_{\rm in}^{(n)}-\zeta_{{\rm out},w}^{(n-1)}). \tag{20}$$

The wave amplitude at the exit from the device,

$$\tilde{\tilde{F}}=\sum_{l=1}^{3}C_l^{(N)}e^{i\gamma_l^{(N)}(\zeta_{\rm out}^{(N)}-\zeta_{\rm in}^{(N)})}$$

(where N is the number of the final stage), determines the gain

$$G=20\log\left\{\left|\sum_{l=1}^{3}C_l^{(N)}e^{i\gamma_l^{(N)}(\zeta_{\rm out}^{(N)}-\zeta_{\rm in}^{(N)})}\right|\right\}. \tag{21}$$

Above, we described the method of solving Eqs. (14)–(16). Certainly, Eqs. (9)–(11) can be solved in a similar manner.

B. Operation near cutoff

In the case of operation near cutoff, both forward and backward waves can be excited by electrons. Superposition of these waves having the same, fixed transverse structure forms an eigenmode of such a circuit. Therefore, instead of considering a forward wave propagating along the axis with the axial wave number k_z, it is necessary to consider the field whose axial structure in a waveguide excited near cutoff frequency is determined by an electron beam [5,20]. Correspondingly, instead of Eqs. (2)–(4), one should use a self-consistent set of equations (cf. Ref. [5]).

$$\frac{dw}{d\zeta}=-2(1-w)^{s/2}\,{\rm Re}(fe^{-i\theta}), \tag{22}$$

$$\frac{d\theta}{d\zeta}=w-\Delta+s(1-w)^{s/2-1}\,{\rm Im}(fe^{-i\theta}), \tag{23}$$

$$\frac{d^2f}{d\zeta^2}+\overline{h^2}f=iI\frac{1}{2\pi}\int_0^{2\pi}(1-w)^{s/2}e^{i\theta}\,d\theta_0. \tag{24}$$

Equations (22) and (23) represent, respectively, Eqs. (2) and (3) reduced for the case of small k_z; correspondingly, now $w=(2/\beta_{\perp 0}^2)[(\gamma_0-\gamma)/\gamma_0]$, $\theta=s(\int_0^\tau \Omega d\tau'+\phi)-\omega t$, $\zeta=(\beta_{\perp 0}^2/2\beta_{z0})(\omega z/c)$, $b=0$, and $\Delta=(2/\beta_{\perp 0}^2)(1-s\Omega_0/\omega)$. Equation (24) is a string equation in which $\overline{h}=(2\beta_{z0}/\beta_{\perp 0}^2)h$ is the normalized axial wave number, and I is the normalized beam current parameter which does not depend on h and relates to I_0 given by Eq. (6) as

$$I=4h\frac{\beta_{z0}}{\beta_{\perp 0}^2}I_0. \tag{25}$$

Note that our limit $h\to 0$ will also cause some simplification in Eq. (6) which determines I_0. Also note that the term $\overline{h}^2$ in Eq. (24) characterizes a small departure from cutoff; however, the field excited near cutoff cannot be associated with one given axial wave number: after making a Fourier transform, this field can be considered [13] as a superposition of plane waves with small (positive and negative) k_z's having a width of the k_z spectrum of the order of $1/L$, where L is the waveguide length.

In the frame of the small-signal theory, we can again linearize these equations with respect to perturbations caused by a small amplitude field, and, introducing

$$\tilde{w}=\frac{1}{f_0}\frac{1}{2\pi}\int_0^{2\pi} w_{(1)}e^{i\theta_0}\,d\theta_0,\quad \tilde{\theta}=\frac{1}{f_0}\frac{1}{2\pi}\int_0^{2\pi}\theta_{(1)}e^{i\theta_0}\,d\theta_0,$$

$$\tilde{f}=\frac{f}{f_0}e^{i\Delta\zeta}, \tag{26}$$

(where f_0 is the field amplitude at the entrance to the first waveguide), reduce Eqs. (22)–(24) to the following set of equations:

$$\frac{d\tilde{w}}{d\zeta}=-\tilde{f}, \tag{27}$$

$$\frac{d\tilde{\theta}}{d\zeta}=\tilde{w}-i\frac{s}{2}\tilde{f}, \tag{28}$$

$$\frac{d^2\tilde{f}}{d\zeta^2}-2i\Delta\frac{d\tilde{f}}{d\zeta}+(\overline{h}^2-\Delta^2)\tilde{f}=iI\left(i\tilde{\theta}-\frac{s}{2}\tilde{w}\right). \tag{29}$$

Here Eqs. (27) and (28) are essentially the same as Eqs. (9) and (10), respectively, while Eq. (29) is more complicated than Eq. (11). Note that the term $\overline{h}^2-\Delta^2$ in Eq. (29) can be represented as

$$-\frac{4}{\beta_{\perp 0}^4\omega^2}(\omega-k_z v_{z0}-s\Omega_0)(\omega+k_z v_{z0}-s\Omega_0),$$

which is the product of cyclotron resonance detunings for forward and backward components of the field.

For perturbations $\tilde{w}$, $\tilde{\theta}$, $\tilde{f}\sim\exp(i\Gamma\zeta)$, Eqs. (27)–(29) yield the fourth-order dispersion equation [21]

$$\Gamma^2(\Gamma^2-2\Delta\Gamma-\overline{h}^2+\Delta^2)+sI\Gamma-I=0. \tag{30}$$

Note that the fourth order of Eq. (30) corresponds to our consideration in which not only two cyclotron beam waves but also forward and backward waveguide waves are taken into account, in contrast to the treatment of operation far from cutoff done in Sec. II A, where the interaction between electrons and backward waves was neglected as nonsynchronous.

When the beam current parameter is small enough ($I^{1/4}\ll 1$) we can introduce $\gamma=\Gamma/I^{1/4}$, $\delta=\Delta/I^{1/4}$, and $\bar{\bar{h}}=\overline{h}/I^{1/4}$ and, ignoring small terms proportional to $I^{1/4}$, reduce Eq. (30) to

$$\gamma^2(\gamma^2-2\delta\gamma+\delta^2-\bar{\bar{h}}^2)=1. \tag{31}$$

This simplified dispersion equation corresponds to reducing Eqs. (27)–(29) to the equations

$$\frac{d\tilde{\tilde{w}}}{d\zeta'}=-\overline{f}, \tag{32}$$

$$\frac{d\tilde{\theta}}{d\zeta'}=\tilde{\tilde{w}}, \tag{33}$$

$$\frac{d^2\overline{f}}{d\zeta'^2}-2i\delta\frac{d\overline{f}}{d\zeta'}+(\bar{\bar{h}}^2-\delta^2)\overline{f}=-\tilde{\theta}, \tag{34}$$

where $\zeta'=\zeta I^{1/4}$, $\tilde{\tilde{w}}=\tilde{w}/I^{1/4}$, and $\overline{f}=\tilde{f}/I^{1/2}$.

In the case of exact cyclotron resonance, $\delta=0$, Eq. (31) yields two roots

$$\gamma_{1,2}=\pm i\left\{\left[1+\left(\frac{\bar{\bar{h}}^2}{2}\right)^2\right]^{1/2}-\frac{\bar{\bar{h}}^2}{2}\right\}^{1/2}. \tag{35}$$

which correspond to the growing and decaying partial waves and two other roots,

$$\gamma_{3,4}=\pm\left\{\left[1+\left(\frac{\bar{\bar{h}}^2}{2}\right)^2\right]^{1/2}-\frac{\bar{\bar{h}}^2}{2}\right\}^{1/2},$$

which correspond to two constant amplitude waves propagating along the axis with slightly different phase velocities. As follows from Eq. (35), the maximum growth rate occurs in the case of operation at the cutoff frequency ($\bar{\bar{h}}\to 0$). Its value $\gamma_{\max}=1$ is a little larger than the maximum growth rate normalized to $I_0^{1/3}$ in the case of operation far from cutoff, which, as follows from Eq. (13), is equal to $\sqrt{3}/2$ [19]. The difference between these two normalizations of the growth rate will be discussed below.

Coming back to Eq. (31), let us note that this equation is more complicated than Eq. (13), not simply because the former is quartic while the latter is cubic, but also because Eq. (31) contains two parameters (δ and $\bar{\bar{h}}$) instead of the one detuning δ in Eq. (13). This corresponds to the above-mentioned necessity of considering (in the case of operation near cutoff) cyclotron resonance with both forward and backward waves.

Representing the field as $\overline{f}=\Sigma_{l=1}^4 C_l e^{i\gamma_l\zeta'}$ we can again find the amplitudes of partial waves, C_l, from equations representing the boundary conditions. For the electron energy

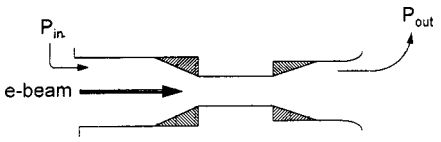

FIG. 1. Schematic of a two-stage device with attenuators.

and phase the boundary conditions are the same as before. For the field, we should also add the condition for the field derivative to the boundary condition for the field amplitude at the entrance to each section, $\overline{f}^{(1)}(0)=1$, $\overline{f}^{(n>1)}(\zeta_{\rm in}^{(n)})=0$. For the first stage, the ingoing boundary condition is

$$\left.\frac{d\overline{f}^{(1)}}{d\zeta'}\right|_0 = i\sum_{l=1}^{4}\gamma_l^{(1)}C_l^{(1)} = -i\bar{\bar{h}}^{(1)}. \tag{36}$$

[In the right-hand side of this equation, we took into account that $\overline{f}^{(1)}(0)=1$.] For the output waveguide we should use the outgoing boundary condition

$$\left.\frac{d\overline{f}^{(N)}}{d\zeta'}\right|_{\zeta_{\rm out}'^{(N)}} = -i\bar{\bar{h}}^{(N)}\overline{f}^{(N)}(\zeta_{\rm out}'^{(N)}),$$

which can be rewritten as

$$\sum_{l=1}^{4}(\gamma_l^{(N)}+\bar{\bar{h}}^{(N)})C_l^{(N)}e^{i\gamma_l^{(N)}(\zeta_{\rm out}^{(N)}-\zeta_{\rm in}^{(N)})}=0. \tag{37}$$

So, for instance, in the case of a two-stage gyro-TWT, the coefficients $C_l^{(1)}$ for the input waveguide are determined by Eqs. (17) and (18) [in which $\tilde{\bar{w}}(0)=\tilde{\bar{\theta}}(0)=0$], [Eq. (36)], and $\overline{f}^{(1)}(0)=\Sigma_{l=1}^{4}C_l^{(1)}=1$. For the output waveguide the coefficients $C_l^{(2)}$ are determined by Eqs. (17) and (18) with nonzero $\tilde{\bar{w}}(\zeta_{\rm in}'^{(2)})$ and $\tilde{\theta}(\zeta_{\rm in}'^{(2)})$ [Eq. (37)] and $\overline{f}^{(2)}(\zeta_{\rm in}'^{(2)})=0$. When the waveguides are ended with some attenuators absorbing the microwave power propagating through the waveguide, any of these waveguides can be subdivided into two parts, as shown in Fig. 1. In the first part, which does not contain a lossy dielectric, the amplitudes of partial waves can be found in the same manner as in the output waveguide (i.e., with the outgoing boundary condition). For the second part, which contains a lossy material, we can use the ingoing boundary condition for the wave amplitude and the dispersion equation (31), in which the parameter $\bar{\bar{h}}$ proportional to the axial wave number is complex in the presence of attenuation. Certainly the same method can be used for analyzing a multistage gyro-TWT operating far from cutoff. The gain can be determined by the same Eq. (21), in which the summation should be done now over four partial waves.

Before closing this subsection, let us emphasize again that the stages may have different parameters. For instance, the difference in transverse dimensions of waveguides changes the axial wave number in each section. Therefore, the detuning Δ in Eq. (12) [or δ, $\overline{h}$, and $\bar{\bar{h}}$ in Eqs. (13), (30), and (31), respectively] can be specific for each stage. In a certain sense, for the bandwidth of the device this difference may play the same role as stagger tuning of eigenfrequencies in the cavities of conventional klystrons [22] or gyroklystrons [23].

C. Two-stage gyro-TWT with tapered parameters

As mentioned in Sec. I, one of the most promising schemes for wide-band operation is a two-stage gyro-TWT, in which cross sections of the input and output waveguides as well as the guiding magnetic field vary along the axis. Such a scheme was studied in Refs. [5–9]. As mentioned in Ref. [6], when the tapering of the waveguides and the magnetic field are matched in such a way that in any cross section the electron cyclotron frequency (or its resonant harmonic) is equal to the cutoff frequency of the operating wave, the system may exhibit a very broadband operation. In this case the interaction is the most efficient in the waveguide sections where the frequency is close to cutoff and the frequency tuning just shifts these interaction regions along the axis. So the bandwidth of such a device is mostly restricted by the electron velocity spread, whose effect increases as the distance between interaction regions grows.

For describing the operation of this device one again can use Eqs. (22)–(24) in which now the cyclotron resonance mismatch Δ and the normalized axial wave number $\overline{h}$ depend on the axial coordinate ζ. In the frame of the small-signal theory these equations can be reduced to one integrodifferential equation,

$$\frac{d^2f}{d\zeta^2}+\overline{h}^2 f = Ir^*\left\{is\int_0^{\zeta} fr\,d\zeta' + \int_0^{\zeta}\int_0^{\zeta'} fr\,d\zeta''d\zeta'\right\}, \tag{38}$$

in which $r=\exp\{i\int_0^{\zeta}\Delta\,d\zeta'\}$. Note that introducing the variables $I'=s^4I$, $\zeta'=\zeta/s$, and $\overline{h'}=s\overline{h}$ allows one to eliminate from Eq. (38) the harmonic number s [5].

To solve Eq. (38) is rather difficult. Also, the axial dependence of $\overline{h}$ and Δ does not allow one to use the simple formalism used above for solving Eqs. (9)–(11), (14)–(16), (27)–(29), and (32)–(34). Therefore, it was suggested in Ref. [6] that the system be analyzed by using the specified-field approximation in the input waveguide and the specified-current approximation in the output waveguide. This assumption was also used in Ref. [8], where the derivation of the expression for the efficiency was shown (in contrast to Ref. [6], where the derivation of this expression was omitted completely). Since an expression for small-signal gain was derived in none of these references, we describe this derivation in the Appendix. The resulting expression for the small-signal gain in the case of linearly tapered magnetic field and waveguide radius is:

$$G=10\log\left\{(2\pi)^4\frac{I_{(2)}^2\zeta_{\rm dr}^2 v^2(\tau_1)v^2(\tau_2)}{\overline{\alpha}_{(1)}^{-1/3}\overline{\alpha}_{(2)}^{-1/3}m_{(1)}m_{(2)}}\right\}. \tag{39}$$

Here $I_{(2)}$ is the normalized beam current parameter determined by Eq. (25) for the output waveguide, $\zeta_{\rm dr}$ is the effective drift length which can be determined as the normalized distance between cutoff cross sections in two waveguides, $\zeta_{\rm dr}=\zeta_{c(2)}-\zeta_{c(1)}$, $v(\tau)$ is the Airy function whose argument is equal to

$$\tau = \frac{\overline{\alpha}^{1/3}}{m}\left(\Delta_c - \frac{\overline{\alpha}}{4m}\right). \tag{40}$$

Here, as in Eq. (39), the coefficients $\overline{\alpha}$ and m characterize the slopes of the waveguide radius and external magnetic field in each waveguide, respectively; as shown in the Appendix, these coefficients correspond to representation of the normalized axial wave number in Eqs. (24) and (38) as

$$\overline{h}^2_{(n)} = (-1)^n \overline{\alpha}_{(n)}(\zeta - \zeta_{c(n)}),$$

and the cyclotron resonance mismatch as

$$\Delta_{(n)} = \Delta_{c(n)} + (-1)^n m_{(n)}(\zeta - \zeta_{c(n)}).$$

Here the index (n) denotes the waveguide section ($n=1$ and 2), and $\Delta_{c(n)}$ is the cyclotron resonance mismatch for the cutoff cross section of the nth waveguide. Note that when the magnetic field tapering corresponds to the tapering of the waveguide wall, this mismatch $\Delta_{c(n)}$ does not depend on the operating frequency. Then the only frequency-dependent term in Eq. (39) is $\zeta_{\rm dr} = \zeta_{c(2)} - \zeta_{c(1)}$, since the cutoff cross section is determined by the frequency. This may lead to a very broadband operation. As pointed out in Ref. [6], in such a device the bandwidth can be restricted by the effect of velocity spread on transit angles through the drift regions. Some estimates done in Ref. [6] for realistic values of spread predicted a 7% bandwidth; also, some calculations done in Ref. [8] showed the possibility of operating in a 27% bandwidth, which is consistent with the 20% bandwidth experimentally demonstrated in Ref. [9].

Note that without making an assumption about the specified-field and specified-current approximations in the input and output waveguides, respectively, one can also develop a small-signal theory of these devices. However, for this general case the theory will be much more complicated. Even a simple attempt to take electron phase bunching in the waveguides into account makes it necessary to integrate Airy functions, which cannot be done analytically, although these integrals are tabulated elsewhere [24].

III. RESULTS

We have studied two-stage traveling-wave amplifiers operating both far from and close to cutoff regimes. The operation far from cutoff is illustrated by Fig. 2, which shows the dependence of the gain on the frequency detuning for a system described by Eqs. (13) and (17)–(19). The calculations are done for the normalized lengths of the first and second waveguides equal to $\zeta'^{(2)}_{\rm out} - \zeta'^{(2)}_{\rm in} = \zeta'^{(1)}_{\rm out} - \zeta'^{(1)}_{\rm in} = 3$ and the normalized length of the drift section $\zeta'^{(2)}_{\rm in} - \zeta'^{(1)}_{\rm out} = 2.5$. The detuning δ shown along the horizontal axis in Fig. 2 is the detuning in the first waveguide. The detuning in the second waveguide is represented as $\delta_2 = \delta + \Delta_d$, where d stands for detuning, so this Δ_d describes the difference in parameters of two stages. As is seen in Fig. 2, as Δ_d increases, the gain becomes smaller; however, the bandwidth can be increased, first, when the gain curve becomes flat, as shown for $\Delta_d = 2.75$, and second, when the gain curve exhibits two peaks of approximately the same amplitude with a relatively small valley between them, as shown for $\Delta_d = 4.8$. Note that the change of sign of Δ_d does not affect the results, since in the frame of the linear theory both stages play a similar role in the amplification process. For the gain curves shown in Fig. 2, the change of sign of Δ_d from plus to minus causes only shift of the curves to the region of larger detunings δ.

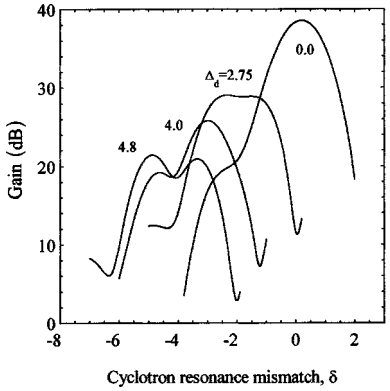

FIG. 2. Gain as a function of the cyclotron resonance mismatch in the input waveguide δ for several values of the detuning parameter Δ_d, characterizing the difference between such mismatches in the input and output waveguides.

The resulting dependence of the maximum gain and bandwidth (the latter is expressed in terms of δ) on the detuning parameter Δ_d is shown in Fig. 3 for the same lengths of all sections. Note that, as the drift section length increases, the second peak in the bandwidth increases and narrows. This bandwidth increase can be explained by the enhancement of electron ballistic bunching in the drift region. The narrowing of this peak follows from the fact that with an increase in drift section length the difference between maximum and minimum values of the gain, like the ones shown in Fig. 2 for $\Delta_d = 4.8$, grows. So, in the limiting case, it is possible to find such values of Δ_d and drift section length for which both peaks are equal and the minimum gain between these peaks is just 3 dB smaller than these maxima. Certainly, in this limiting case, any variation in Δ_d will make the gain deviation larger than 3 dB, thus reducing the bandwidth. Note that in the region of such a narrow peak, the gain (21.4 dB) is much smaller than for $\Delta_d = 0$, when $G = 38.5$ dB. Therefore, in terms of the gain-bandwidth product, it is preferable to operate in the vicinity of the first peak: for instance, for $\Delta_d = 0$, 2.75, and 4.8, this product (when the gain is expressed

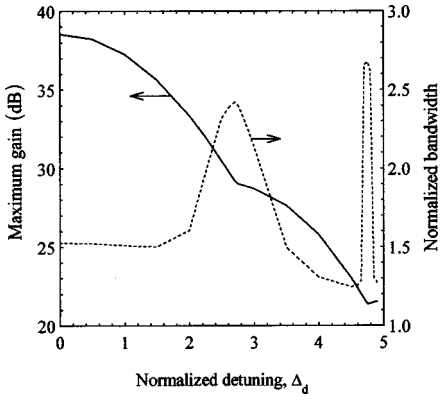

FIG. 3. Maximum gain and normalized bandwidth as functions of the detuning parameter Δ_d.

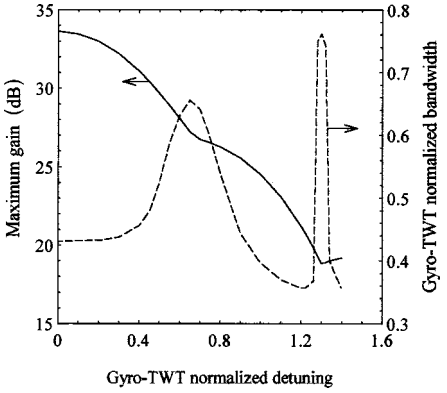

FIG. 4. Maximum gain and normalized bandwidth calculated with the account for *M*-type interaction effects.

in dB and the bandwidth in δ) is equal to 58.5, 70.2, and 57.3, respectively. (Below we will discuss the correspondence between δ and the real bandwidth.)

The results shown in Figs. 2 and 3 are valid for the linear beam TWT and the gyro-TWT, in which some small terms proportional to $I_0^{1/3}$ are ignored. To check the importance of these terms for gyro-TWT operation, we have studied a more complete set of equations, i.e., Eq. (12) and boundary conditions for $\tilde{w}$, $\tilde{\theta}$, and $\tilde{F}$, which follow from Eqs. (9)–(11) for $I_0=0.0234$. (This value of I_0 will be motivated below.) The results are shown in Fig. 4, which is similar to Fig. 3. Note that the normalized detuning along the horizontal axis and the bandwidth shown in Fig. 4 correspond, respectively, to the detuning and bandwidth shown in Fig. 3, multiplied by $I_0^{1/3}\simeq 0.286$. Both figures are very similar; however, the effects of *M*-type interaction [13,15,18] ignored in previous analyses leads to a certain degradation in gain. The latter analysis was done for the case of interaction in both stages at the fundamental cyclotron resonance. (Recall that, in the theory of gyrodevices, the *M*-type effects in electron bunching and coherent radiation and absorption are associated with a ''direct'' action of the wave upon electrons [13,15,18]. Such a bunching occurs only in the process of interaction, in contrast to *O*-type effects caused by the relativistic dependence of the electron gyrofrequency on its energy. The latter effects leading to electron orbital bunching may proceed in a drift region that is free from microwaves after initial modulation of electron energies in the input stage of the device.)

In the rest of this section we present the results of the study of near cutoff operation. The roots of Eq. (31) are shown in Figs. 5(a), 5(b), 5(c), and 5(d) for $\bar{\bar{h}}=0$, 1, 2 and 3, respectively. As follows from these figures, the increase in $\bar{\bar{h}}$, which means a departure from cutoff operation, reduces the growth rate of the growing wave, and simultaneously stretches the region of cyclotron resonance mismatches in which the amplification occurs.

The operation of the gyro-TWT with two identical waveguides is illustrated by Figs. 6 and 7. In Fig. 6, the gain curves are shown for several values of the parameter $\bar{\bar{h}}$; the normalized lengths of the sections are equal to $\zeta'^{(1)}_{\rm out}-\zeta'^{(1)}_{\rm in}=\zeta'^{(2)}_{\rm out}-\zeta'^{(2)}_{\rm in}=2.5$ and $\zeta'_{\rm dr}=\zeta'^{(2)}_{\rm in}-\zeta'^{(1)}_{\rm out}=1$. These gain curves, as well as those which are not shown in Fig. 6, demonstrate a strong dependence of the gain and bandwidth on the parameter $\bar{\bar{h}}$: the device exhibits a low-gain, large-bandwidth operation when $\bar{\bar{h}}$ is smaller than 0.6, close to 1, or between 1.5 and 1.9, while at $\bar{\bar{h}}$ of close to 0.75, in the region of 1.15–1.4, and between 1.9 and 2, the gain is high and the bandwidth is narrow. These results are summarized in Fig. 7, which shows four sharp peaks in the gain as a

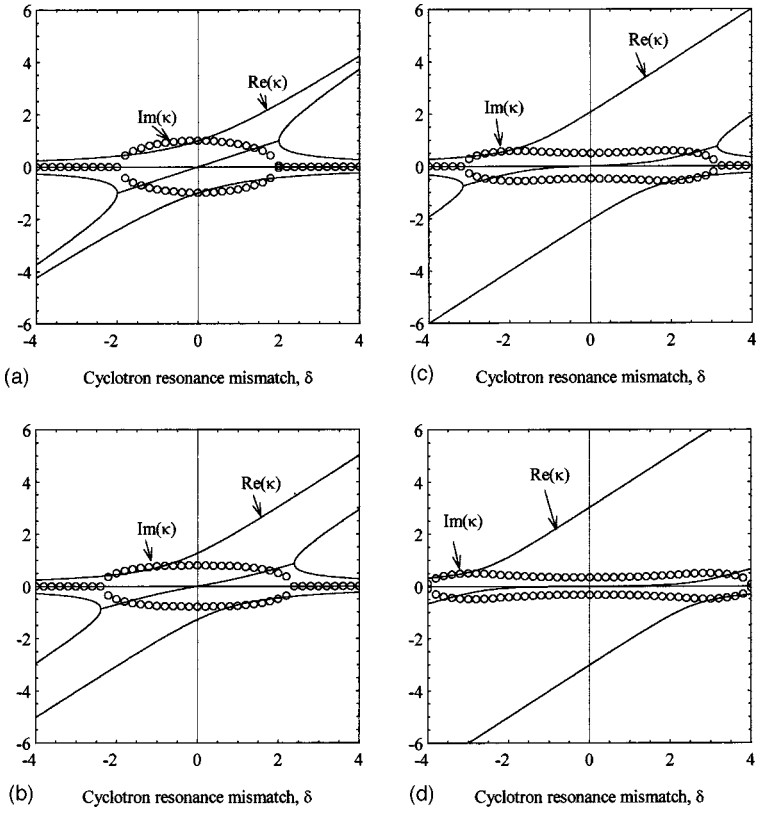

FIG. 5. Roots of the dispersion equation describing the operation near cutoff; circles show growth rates, solid lines show propagation constants. (a), (b), (c), and (d) correspond, respectively, to a normalized axial wave number $\bar{\bar{h}}$ equal to 0, 1, 2, and 3.

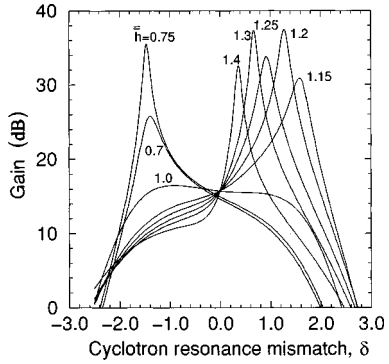

FIG. 6. Gain as a function of the cyclotron resonance mismatch for the case of operation near cut-off in a two-stage gyro-TWT with equal cutoff frequencies of both waveguides.

function of $\bar{h}$ and the large bandwidths in the valley between the first two peaks and in the valley between the last two peaks. Note that the largest gain-bandwidth product corresponds to the operation in the first valley.

The effect of ''stagger tuning,'' i.e., the operation of two waveguides at different values of $\bar{h}$, is illustrated by Figs. 8(a) and 8(b), which correspond to $\tilde{h}=0.6$ and -0.6, respectively. Here $\tilde{h}=\bar{h}^{(2)}-\bar{h}^{(1)}$. These figures look very similar to Fig. 7, although the curves are shifted along the horizontal axis, which shows the value of $\bar{h}^{(1)}$, corresponding to the value of $\tilde{h}$. In all three cases the maximum values of the gain in sharp, narrow peaks are about 50–60 dB and the decrease in the gain is usually accompanied by an increase in the bandwidth. Note that the maximum bandwidth corresponds to $\tilde{h}=-0.6$; see the first valley in the gain curve shown in Fig. 8(b). Also important are plateaus in the bandwidth shown in Figs. 7 and 8(b) for relatively large axial wave numbers. These plateaus are important since the frequency deviation within the bandwidth causes some changes in the axial wave number. So, strictly speaking, correct calculations of the bandwidth would be done for the specified ratio of the carrier frequency to the cutoff frequency and for the specific electron cyclotron frequency. Then variation of the frequency within the bandwidth should be taken into account in the detuning δ and axial wave number $\bar{h}$, simultaneously.

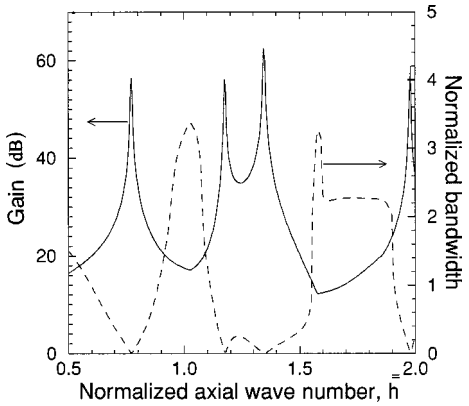

FIG. 7. Maximum gain and normalized bandwidth as functions of the normalized axial wave number $\bar{h}$ in a two-stage gyro-TWT with equal cutoff frequencies of both waveguides.

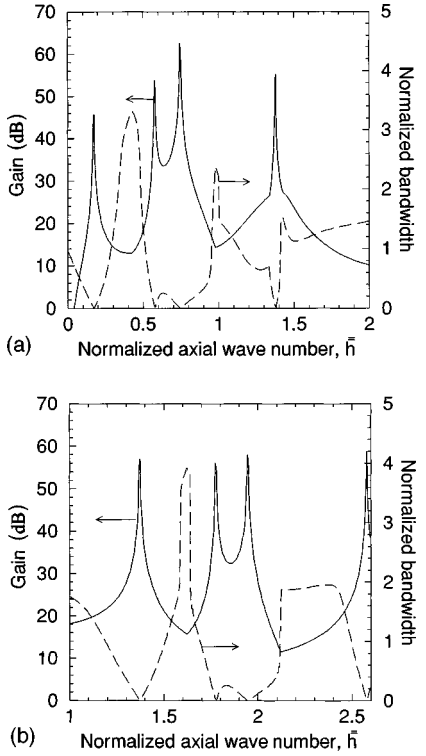

FIG. 8. Maximum gain and normalized bandwidth as functions of the normalized axial wave number in the first waveguide, $\bar{h}^{(1)}$, for a detuning $\overline{h}=\bar{h}^{(2)}-\bar{h}^{(1)}$ equal to 0.6 (a) and -0.6 (b).

Since in our calculations we ignored this effect, the bandwidth shown in Figs. 7 and 8 should be considered only as an illustration.

IV. DISCUSSION

Let us discuss the relation between the normalized parameters used in our treatment and the real parameters of concrete devices. Consider a two-stage gyro-TWT operating at the fundamental cyclotron resonance, in which a TE_{01} wave of cylindrical waveguides is excited by an 80-kV, 2-A electron beam with an orbital-to-axial velocity ratio of $\alpha=1.3$. Assume that a thin annular electron beam has a radius corresponding to the maximum coupling to the TE_{01} wave at the fundamental harmonic [in Eq. (7), $k_\perp R_0=1.84$]. For the coupling impedance given by Eq. (7) this yields the value $G_{\mathrm{cpl}}\simeq 0.42$. The velocity components for a given beam voltage and $\alpha\simeq 1.3$ are approximately equal to $\beta_{\perp 0}\simeq 0.4$ and $\beta_{z0}\simeq 0.3$. Correspondingly, the normalized beam current parameter I present in Eqs. (24) and (29) is equal to 0.0177, and the normalized current parameter I_0, which is determined by Eq. (16), is equal to $0.00234/h$. So, for instance, when the axial wave number is equal to $0.1(\omega/c)$, $I_0=0.0234$, and $I_0^{1/3}$, which plays the role of the Pierce gain parameter, is equal to 0.286. This is just the value used in calculations, the results of which are shown above in Fig. 4. Note that in the case of operation near cutoff, the role of the Pierce gain parameter is played by $I^{1/4}$, which in our example is equal to 0.365. These powers of normalized current

parameters also determine the growth rates of the waves in the cases of operation far from and close to cutoff.

Let us start by considering operation far from cutoff in the case of exact cyclotron resonance. Equation (13) for $\Delta=0$ yields the maximum growth rate $\mathrm{Im}\,\gamma=\sqrt{3}/2$, which for the propagation constant Γ present in Eq. (12) corresponds to $\mathrm{Im}\,\Gamma=(\sqrt{3}/2)I_0^{1/3}\approx 0.25$. This means that the exponential growth of the wave occurs at distance $\zeta_{\mathrm{exp}}\sim(\mathrm{Im}\,\Gamma)^{-1}\simeq 4$, which corresponds to $L_{\mathrm{exp}}/\lambda\simeq 2.4$. Note that the results shown in Figs. 2 and 3 correspond to the distance multiplied by $I_0^{1/3}$; i.e., the normalized length of each waveguide taken equal to 3 in those calculations is 2.6 times larger than the exponential length $(\mathrm{Im}\,\gamma)^{-1}$. In other words, the length of each waveguide is close to 6λ. The bandwidth, which in the normalized units used in Figs. 2 and 3, can be about 2.5, for $\beta_{\perp 0}\simeq 0.4$ and $I_0^{1/3}\simeq 0.286$ corresponds to the bandwidth, $\Delta f/f=5.67\%$.

In a similar way, consider operation near cutoff. In the limiting case of exact cyclotron resonance and operation very close to cutoff, Eq. (35) yields the growth rate $\mathrm{Im}\,\gamma=1$, which is equivalent to $\mathrm{Im}\,\Gamma=I^{1/4}$. In our example, this means $\mathrm{Im}\,\Gamma=0.365$. Correspondingly, the distance at which the wave amplitude increases by e times is equal to $\zeta_{\mathrm{exp}}\sim(\mathrm{Im}\,\Gamma)^{-1}\simeq 2.74$, which corresponds to $L_e/\lambda\simeq 1.65$. So, the growth rate in this case is a little higher than in the previously considered case of operation at the wave with $k_z=0.1\omega/c$.

ACKNOWLEDGMENTS

The authors would like to thank Dr. A. K. Ganguly and Dr. M. A. Moiseev for useful discussions of issues presented in Sec. II C and the Appendix. This work was supported by the U.S. Office of Naval Research and by the DOD MURI program on High-Power Microwaves.

APPENDIX: SMALL-SIGNAL GAIN IN A TWO-STAGE TAPERED GYRO-TWT

Consider a two-stage gyro-TWT in which the input waveguide is linearly down-tapered and the external magnetic field there is linearly up-tapered while the output waveguide is linearly up-tapered and the magnetic field there is linearly down-tapered to maintain the cyclotron resonance condition. These two tapered waveguide sections can be separated by a waveguide of a constant radius, which is below cutoff for all operating frequencies.

The linear tapering of the waveguides allows one to represent the squared normalized axial wave number $\overline{h^2}$ in Eq. (24) as

$$\overline{h^2_{(n)}}=(-1)^n\overline{\alpha}_{(n)}(\zeta-\zeta_{c(n)}), \tag{A1}$$

where n is the stage number, and $\overline{\alpha}_{(n)}=2(2\beta_{z0}/\beta_{\perp 0}^2)(\alpha_{(n)}/\nu_{(n)})$ is the parameter of wall tapering for the nth stage. Here $\nu_{(n)}$ is the eigennumber of the operating mode in the nth stage, and $\alpha_{(n)}$ describes a small slope of the cylindrical waveguide radius: $\alpha_{(1)}=(R_{\mathrm{in}}-R_{\mathrm{min}})/L_1$ and $\alpha_{(2)}=(R_{\mathrm{out}}-R_{\mathrm{min}})/(L_{\mathrm{out}}-L_2)$; R_{in}, R_{out}, and R_{min} are, respectively, the input and output radii, and the minimum radius, which is the radius of a straight section between two tapered waveguides; L_1 is the length of the first waveguide; L_2-L_1 is the length of the straight section; and L_{out} designates the end of the output waveguide. Also in Eq. (A1), $\zeta_{c(n)}$ is the coordinate of the cutoff cross section, which depends on the operating frequencies: $\zeta_{c(1)}=(\beta_{\perp 0}^2/2\beta_{z0})[\omega(R_{\mathrm{in}}-\nu c/\omega)/\alpha_{(1)}c]$ and $\zeta_{c(2)}=\zeta_{\mathrm{in}}^{(2)}+(\beta_{\perp 0}^2/2\beta_{z0})[\omega(\nu c/\omega-R_{\mathrm{min}})/\alpha_{(2)}c]$.

The tapering of the magnetic field in the case when we keep the cyclotron frequency (or its resonant harmonic) equal to the cutoff frequency for any ω should correspond to the wall tapering:

$$B_0(\zeta)=B_0(\zeta_c)R(\zeta_c)/R(\zeta).$$

Correspondingly, the cyclotron resonance mismatch in both tapered waveguides can be determined as

$$\Delta_{(n)}=\Delta_{c(n)}+(-1)^n m_{(n)}(\zeta-\zeta_{c(n)}), \tag{A2}$$

where $\Delta_{c(n)}=(2/\beta_{\perp 0}^2)[\omega-s_{(n)}\Omega_0(z_{c(n)})]/\omega$ is the cyclotron resonance mismatch for the cutoff cross section (its coordinate $z_{c(n)}$ corresponds to $\zeta_{c(n)}$ defined above), and

$$m_{(n)}=4(\beta_{z0}/\beta_{\perp 0}^4)(\alpha_{(n)}/\nu_{(n)})(\omega_{c(n)}/\omega)$$
$$\simeq 4(\beta_{z0}/\beta_{\perp 0}^4)(\alpha_{(n)}/\nu_{(n)})$$

describes the effect of magnetic field tapering.

Assuming the specified-field approximation for the input waveguide, we can represent the field f as $Af_{(0)}(\zeta)$, where the amplitude A is determined by the power of a driver, P_{dr} [25]: $A^2=4I_1P_{\mathrm{dr}}/P_{0\perp}$ (here $P_{0\perp}$ is the beam power associated with electron gyration). The ''cold-cavity'' function $f_{(0)}(\zeta)$ is determined by Eq. (24), in which the beam effects, i.e., its right-hand side (RHS), is ignored. Taking Eq. (A1) into account, this equation can be rewritten as

$$\frac{d^2f_{(0)}}{d\zeta^2}-\overline{\alpha}_{(1)}(\zeta-\zeta_{c(1)})f_{(0)}=0.$$

Introducing the variable $t=\overline{\alpha}_{(1)}^{1/3}(\zeta-\zeta_{c(1)})$ we can transform this equation into the known Airy equation

$$\frac{d^2f_{(0)}}{dt^2}=tf_{(0)}, \tag{A3}$$

the solution to which is the superposition of two Airy functions: $f_{(0)}=B_1u(t)+B_2v(t)$. To eliminate the divergence of this solution at $t\to\pm\infty$, we should assume $B_1=0$. Also, since the wave amplitude is determined by A, we will assume $B_2=1$, which yields $f_{(0)}=v(t)$ [26].

Using this representation of the field, one can integrate linearized equations for electron motion [Eqs. (22) and (23)]. Below, we will assume that the interaction regions in both tapered waveguides are much shorter than the drift space between them. This allows us, first, to determine the modu-

lation in electron energies in the first tapered waveguide, and then to calculate the orbital phase bunching in the drift region caused by this modulation. As follows from Eq. (22), the energy modulation is equal to

$$w_{(1)}(\zeta_{\rm out}^{(1)}) = -\frac{2A}{\overline{\alpha}_{(1)}^{1/3}} \mathrm{Re}\left\{ e^{-i\theta_0} \int_{t_{\rm in}^{(1)}}^{t_{\rm out}^{(1)}} \hat{v}\, dt \right\}, \tag{A4}$$

where $\hat{v}(t) = v(t)\exp\{i\int_0^\zeta \Delta_{(1)}\, d\zeta'\}$, and $\Delta_{(1)}$ is given by Eq. (A2).

To calculate the integral on the RHS of Eq. (A4), let us use the integral representation of the Airy function [25]:

$$v(t) = \frac{1}{\sqrt{\pi}} \int_0^\infty \cos\left(\frac{x^3}{3} + xt \right) dx = \frac{1}{2\sqrt{\pi}} \int_{-\infty}^{\infty} e^{i[(x^3/3)+xt]}\, dx. \tag{A5}$$

This leads to the necessity to calculate the integral

$$F_{(1)} = \int_{-\infty}^{\infty} \hat{v}\, dt = \frac{1}{2\sqrt{\pi}} \int_0^\infty \left\{ \int_{-\infty}^{\infty} e^{i[(x^3/3)+xt+(\Delta_{c(1)}+m_{(1)}\zeta_{c(1)})\zeta-(m_{(1)}/2)\zeta^2]} dx \right\} dt. \tag{A6}$$

Here we replaced the limits of integration $t_{\rm in}^{(1)}$ and $t_{\rm out}^{(1)}$ by $\pm\infty$, assuming that the waveguide is long enough. Representing the variables t and x as $t' + (\overline{\alpha}_{(1)}^{2/3}/m_{(1)})(x + \Delta_{c(1)}/\overline{\alpha}_{(1)}^{1/3})$ and $x' - \overline{\alpha}_{(1)}^{2/3}/2m_{(1)}$, respectively, one can rewrite Eq. (A6) as

$$F_{(1)} = e^{-iC_1} \int_{-\infty}^{\infty} e^{i[(x'^3/3)+x'\tau_1]}\, dx' \int_{-\infty}^{\infty} e^{-i(m_{(1)}/2\overline{\alpha}_{(1)}^{2/3})t'^2}\, dt', \tag{A7}$$

where $C_1 = \overline{\alpha}_{(1)}^2/3(2m_{(1)})^3 - (\overline{\alpha}_{(1)}/2m_{(1)} - \Delta_{c(1)})^2/2m_{(1)} - \Delta_{c(1)}\zeta_{c(1)} - m_{(1)}\zeta_{c(1)}^2/2$ is the phase constant, and

$$\tau_1 = \frac{\overline{\alpha}_{(1)}^{1/3}}{m_{(1)}} \left(\Delta_{c(1)} - \frac{\overline{\alpha}_{(1)}}{4m_{(1)}} \right). \tag{A8}$$

In Eq. (A7) the first integral, as follows from Eq. (A5), is equal to $2\sqrt{\pi}v(\tau_1)$ and the second integral is equal to $\overline{\alpha}_{(1)}^{1/3}\sqrt{\pi/m_{(1)}}(1-i)$. (In finite limits the latter integral would yield a superposition of Fresnel integrals.) As a result, the electron energy modulation given by Eq. (A4) can be represented as

$$w_{(1)}(\zeta_{\rm out}^{(1)}) = -2\left(\frac{\pi}{m_{(1)}} \right)^{1/2} A\, \mathrm{Re}\{ e^{-i(\theta_0+C_1)}(1-i)v(\tau_1) \}. \tag{A9}$$

In accordance with Eq. (23), this energy modulation leads to phase bunching, which at the entrance to the output waveguide will be equal to

$$\theta_{(1)}(\zeta_{\rm in}^{(2)}) = w_{(1)}(\zeta_{\rm out}^{(1)})(\zeta_{\rm in}^{(2)} - \zeta_{\rm out}^{(1)}). \tag{A10}$$

Assuming the specified current approximation to be valid for the output waveguide, we can describe the excitation of this waveguide by a simplified Eq. (24):

$$\frac{d^2 f_2}{d\zeta^2} + \overline{\alpha}_{(2)}(\zeta - \zeta_{c(2)}) f_2 = iI_{(2)} \frac{1}{2\pi} \int_0^{2\pi} e^{i(\theta_0 - \int_0^\zeta \Delta_{(2)}\, d\zeta')} \times \left[-\frac{s}{2} w_{(1)}(\zeta_{\rm out}^{(1)}) + i\theta_{(1)}(\zeta_{\rm in}^{(2)}) \right] d\theta_0. \tag{A11}$$

In variables $\tilde{w}$ and $\tilde{\theta}$ given by Eqs. (26) (in which we assume $f_0 = A$),

$$\tilde{w}(\zeta_{\rm out}^{(1)}) = -\left(\frac{\pi}{m_{(1)}} \right)^{1/2} e^{-iC_1}(1-i)v(\tau_1),$$
$$\tilde{\theta}(\zeta_{\rm in}^{(2)}) = \tilde{w}(\zeta_{\rm out}^{(1)})\zeta_{\rm dr}, \tag{A12}$$

where $\zeta_{dr} = \zeta_{\rm in}^{(2)} - \zeta_{\rm out}^{(1)}$. Correspondingly, Eq. (A11) can be rewritten as

$$\frac{d^2 f}{dt^2} - tf = B\varphi(t), \tag{A13}$$

where the output waveguide field is normalized to A, $t = -\overline{\alpha}_{(2)}^{1/3}(\zeta - \zeta_{c(2)})$,

$$B = -(I_{(2)}/\overline{\alpha}_{(2)}^{2/3})(\zeta_{\rm dr} + is/2)\tilde{w}(\zeta_{\rm out}^{(1)}),$$

and $\varphi = \exp\{-i\int_{\zeta_{\rm in}^{(2)}}^{\zeta} \Delta_{(2)} d\zeta'\}$. A general solution of the inhomogeneous equation (A13) is (see, e.g., Ref. [27])

$$f = u(t)\left[C_1 - \frac{B}{W} \int_{t_{\rm in}}^{t} \varphi(t')v(t')dt' \right] + v(t)\left[C_2 + \frac{B}{W} \int_{t_{\rm in}}^{t} \varphi(t')u(t')dt' \right], \tag{A14}$$

where the Wronskian W for the properly normalized Airy functions is equal to 1 [26]. Here again, in order to avoid singularities at the entrance, $t = t_{\rm in}$, we should assume C_1

$=0$. Then the constant C_2 can be determined from the demand that at the output, $t=t_{\rm out}$, the field should represent an outgoing traveling wave:

$$f(t_{\rm out})=\mathcal{D}[u(t_{\rm out})-iv(t_{\rm out})]. \tag{A15}$$

The fact that such a superposition represents an outgoing forward wave follows from the integral representation of the function $v(t)$ given by Eq. (A5) and the function $u(t)$:

$$u(t)=\frac{1}{\sqrt{\pi}}\int_0^\infty\left[e^{-(x^3/3)+tx}+\sin\left(\frac{x^3}{3}+tx\right)\right]dx,$$

where, for $t=t_{\rm out}\to-\infty$, the first term can be neglected. So

$$f(t_{\rm out})=-i\mathcal{D}\int_0^\infty e^{i[(x^3/3)+t_{\rm out}x]}dx. \tag{A16}$$

From comparison of the first term in Eq. (A14) for $f(t_{\rm out})$ and $C_1=0$ with the first term on the RHS of Eq. (A15), it follows that $\mathcal{D}=-B\int_{t_{\rm in}}^{t_{\rm out}}\varphi(t)v(t)dt$. Then the comparison of the last two terms in these equations yields

$$C_2=-B\int_{t_{\rm in}}^{t_{\rm out}}\varphi(t)[u(t)-iv(t)]dt.$$

Correspondingly, the field at the exit can be determined as

$$f(t_{\rm out})=iB\int_0^\infty e^{i[(x^3/3)+t_{\rm out}x]}\,dx\int_{t_{\rm in}}^{t_{\rm out}}\varphi(t)v(t)dt. \tag{A17}$$

Here the first integral, as follows from Eqs. (A15) and (A16), is just an integral representation of the superposition of two Airy functions, so

$$\int_0^\infty e^{i[(x^3/3)+t_{\rm out}x]}\,dx=\sqrt{\pi}[v(t_{\rm out})+iu(t_{\rm out})]. \tag{A18}$$

The second integral in Eq. (A17) is the complex conjugate to the function $F_{(1)}$ determined by Eqs. (A6) and (A7), in which index (1) should be replaced by index (2). So,

$$\int_{t_{\rm in}}^{t_{\rm out}}\varphi(t)v(t)dt=F^*_{(2)}=e^{iC_2}2\sqrt{\pi}v(\tau_2)\bar{\alpha}_{(2)}^{-1/3}\left(\frac{\pi}{m_{(2)}}\right)^{1/2}\times(1+i). \tag{A19}$$

Correspondingly, the wave intensity at the output can be determined as

$$|f(t_{\rm out})|^2=|B|^2\frac{(2\pi)^3}{\sqrt{|t_{\rm out}|}}\frac{\bar{\alpha}_{(2)}^{2/3}}{m_{(2)}}v^2(\tau_2), \tag{A20}$$

where for $v(t_{\rm out})$ and $u(t_{\rm out})$ we used asymptotic expressions valid for large negative arguments, and $|B|^2$, as follows from the definition of B and Eq. (A12), is equal to

$$|B|^2=\frac{I_{(2)}^2}{\bar{\alpha}_{(2)}^{4/3}}\zeta_{\rm dr}^2\frac{2\pi}{m_{(1)}}v^2(\tau_1). \tag{A21}$$

Substituting Eq. (A21) into Eq. (A20), one obtains

$$|f(t_{\rm out})|^2=\frac{(2\pi)^4I_{(2)}^2\zeta_{\rm dr}^2}{\bar{\alpha}_{(2)}^{2/3}m_{(1)}m_{(2)}\sqrt{|t_{\rm out}|}}v^2(\tau_1)v^2(\tau_2). \tag{A22}$$

Recall that this field is already normalized to the input amplitude in accordance with Eq. (26). Therefore, taking into account that the input and output powers are also proportional to the axial wave numbers in corresponding cross sections, one can easily obtain the following expression for the gain:

$$G=10\log\left\{(2\pi)^4\frac{I_{(2)}^2\zeta_{\rm dr}^2v^2(\tau_1)v^2(\tau_2)}{\bar{\alpha}_{(1)}^{-1/3}\bar{\alpha}_{(2)}^{-1/3}m_{(1)}m_{(2)}}\right\}, \tag{A23}$$

which is essentially the same as one mentioned in Ref. [7]. Note that in Ref. [7] it was suggested that $\zeta_{\rm dr}$ be interpreted as the distance between cutoff cross sections in both waveguides, which makes this value frequency dependent.

[1] K. R. Chu, L. R. Barnett, W. K. Lau, L. M. Chang, and H. Y. Chen, IEEE Trans. Electron. Devices **37**, 1557 (1990).

[2] Y. Y. Lau, K. R. Chu, L. R. Barnett, and V. L. Granatstein, Int. J. Infrared Millim. Waves **2**, 373 (1981).

[3] V. L. Granatstein, M. E. Read, and L. R. Barnett, in *Infrared and Millimeter Waves*, edited by K. J. Button (Academic, New York, 1984), Vol. 5, Chap. 5.

[4] L. R. Barnett, L. H. Chang, H. Y. Chen, K. R. Chu, W. K. Lau, and C. C. Tu, Phys. Rev. Lett. **63**, 1062 (1989).

[5] V. L. Bratman, M. A. Moiseev, M. I. Petelin, and R. E. Erm, Izv. Vyssh. Uchebn., Zaved. Radiofiz. **16**, 622 (1973) [Radiophys. Quantum Electron. **16**, 474 (1973)].

[6] M. A. Moiseev, Izv. Vyssh. Uchebn, Zaved. Radiofiz. **20** 1218 (1977) [Radiophys. Quantum Electron. **20**, 846 (1977)].

[7] A. K. Ganguly and S. Ahn, Int. J. Electron. **53**, 641 (1982).

[8] A. K. Ganguly and S. Ahn, IEEE Trans. Electron Devices **ED-31**, 474 (1984).

[9] G. S. Park, J. J. Choi, S. Y. Park, C. M. Armstrong, A. K. Ganguly, R. H. Kyser, and R. K. Parker, Phys. Rev. Lett. **74**, 2399 (1995).

[10] K. R. Chu, L. R. Barnett, W. K. Lau, L. H. Chang, and C. S. Kou, in *Technical Digest of IEDM* (IEEE, New York, 1990), p. 699.

[11] A. W. Fliflet, Int. J. Electron. **61**, 1049 (1986).

[12] G. S. Nusinovich and H. Li, Int. J. Electron. **72**, 895 (1992).

[13] M. I. Petelin and V. K. Yulpatov, Izv. Vyssh. Uchebn., Zaved. Radiofiz. **18**, 290 (1975) [Radiophys. Quantum Electron. **18**, 212 (1975)].

[14] G. S. Nusinovich and M. Walter, Phys. Plasmas **4**, 3394 (1997).

[15] A. V. Gaponov, Izv. Vyssh. Uchebn., Zaved. Radiofiz. **4**, 547 (1961).

[16] N. S. Ginzburg, I. G. Zarnitsyna, and G. S. Nusinovich, Izv. Vyssh. Uchebn., Zaved. Radiofiz. **24**, 481 (1981) [Radiophys.

Quantum Electron. **24**, 331 (1981)].
[17] V. L. Bratman, N. S. Ginzburg, G. S. Nusinovich, M. I. Petelin, and P. S. Strelkov, Int. J. Electron. **51**, 541 (1981).
[18] V. K. Yulpatov, Izv. Vyssh. Uchebn., Zaved. Radiofiz. **10**, 471 (1967) [Radiophys. Quantum Electron. **10**, 471 (1967)].
[19] J. R. Pierce, *Traveling Wave Tubes* (Van Nostrand, Princeton, 1950).
[20] A. W. Fliflet, M. E. Read, K. R. Chu, and R. Seeley, Int. J. Electron. **53**, 505 (1982).
[21] V. L. Bratman and M. A. Moiseev, Izv. Vyssh. Uchebn., Zaved. Radiofiz. **18**, 1045 (1975) [Radiophys. Quantum Electron. **18**, 772 (1975)].
[22] A. Staprans, E. W. McCune, and J. A. Ruetz, Proc. IEEE **61**, 299 (1973).
[23] G. S. Nusinovich, B. G. Danly, and B. Levush, Phys. Plasmas **4**, 469 (1997).
[24] *Handbook of Mathematical Functions*, edited by M. Abramovitz and I. A. Stegun, Natl. Bur. Stand. U.S. Appl. Math. Ser. No. 55 (U.S. GPO, Washington, DC, 1964), p. 478.
[25] V. S. Ergakov and M. A. Moiseev, Izv. Vyssh. Uchebn., Zaved. Radiofiz. **18**, 120 (1975) [Radiophys. Quantum Electron. **18**, 89 (1975)].
[26] V. A. Fok, *Electromagnetic Diffraction and Propagation Problems* (Pergamon, New York, 1965) Appendix 2.
[27] P. M. Morse and H. Feshbach, *Methods of Theoretical Physics* (McGraw-Hill, New York, 1953), pp. 523–530.